30 March 2001

ELSEVIER

Chemical Physics Letters 337 (2001) 31–35

CHEMICAL PHYSICS LETTERS

www.elsevier.nl/locate/cplett

Carbon nanotubes: A thermoelectric nano-nose

Clement K.W. Adu, Gamini U. Sumanasekera, Bhabendra K. Pradhan, Hugo E. Romero, Peter C. Eklund *

Department of Physics, The Pennsylvania State University, 104 Davey Laboratory, University Park, PA 16802-6300, USA

Received 11 December 2000

Abstract

A thermoelectric 'nano-nose' has been built from tangled bundles of single-walled carbon nanotubes (SWNT). The response is specific to the details of the interaction of the adsorbed molecule with the nanotube wall; even gases such as He, N_2 and H_2 can be easily detected. Plots of ΔS vs. ρ_a are sensitive to whether oxidation or reduction of the tube wall is taking place, and to whether the gas molecule is physisorbed or chemisorbed.

A single-walled carbon nanotube (SWNT) can be envisioned as a monolayer graphene sheet rolled up into a long seamless cylinder [1]. First reported in the products of an electric arc in 1993 by research scientists in NEC-Tsukuba [2] and IBM-Almaden [3], and later produced in much more significant quantities and higher purity by pulsed laser vaporization at Rice University [4], these molecular filaments are now under active investigation for a variety of fundamental reasons, as well as potential new technologies [5]. Both the electric arc and the laser produce well-ordered, tightly packed bundles of tubes containing tens to hundreds of SWNTs [6,4]. Within a bundle, the tubes are bound together by a weak van der Waals force. If all the allowed helicities are statistically populated, a random distribution of ~1/3 metallic tubes and ~2/3 semiconducting tubes would exist in a macroscopic sample [1]. For the tube diameters found in our samples, previous scanning tunneling microscopy [7], optical absorption spectroscopy [8,9] and theoretical calculations [10] report that the semiconducting gap $E_{gap} \sim 0.6$ eV. Similar to graphite, SWNTs are amphoteric [11,12]. That is, they can be doped by electron donors or acceptors that attach to the tube wall, removing or adding electrons to the carbon π electron conduction bands.

The bundle structure of SWNTs produces at least four distinct sites in which gas molecules can adsorb (see Fig. 1): on the external bundle *surface*, in a *groove* formed at the contact between adjacent tubes on the outside of the bundle, within an interior *pore* of an individual tube, and inside an interstitial *channel* formed at the contact of three tubes in the bundle interior. For a particular gas molecule, some of these sites can be excluded on size considerations alone (assuming the bundle or tube does not swell to accommodate the adsorbed molecule). For hydrogen, calculations ignoring swelling have ordered the binding energy (E_B) in these various sites (cf. Fig. 1) as E_B (channels) > E_B (grooves) > E_B (pores) > E_B (surface) [13,14]. Access of molecules to the internal tube pores is

* Corresponding author. Fax: +1-814-865-9851.
E-mail address: pce3@psu.edu (P.C. Eklund).

0009-2614/01/$ - see front matter
PII: S0009-2614(01)00159-2

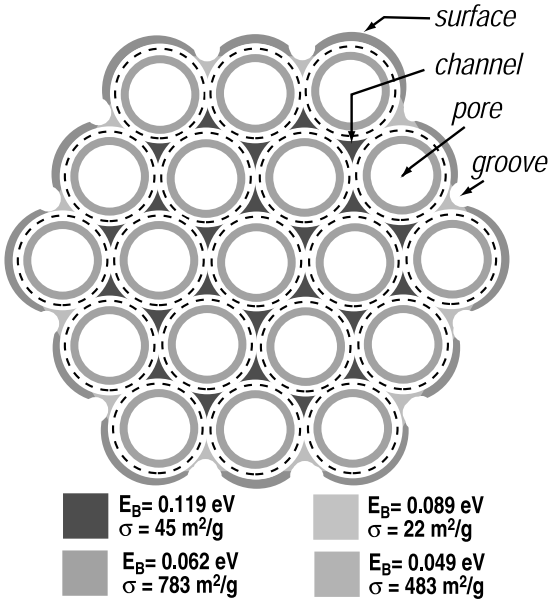

Fig. 1. Schematic structure of a SWNT bundle showing the pore, groove, channel and surface sites available for gas adsorption. Dashed line indicates the nuclear skeleton of the nanotubes. Binding energies (E_B) and specific surface area contributions (σ) for hydrogen adsorption on these sites are indicated [13].

either through open SWNT ends, or defects (holes) in the tube walls. Recently, values exceeding 4 wt% hydrogen have been reported for SWNTs [15–17], even at ambient temperature and pressure [18], suggesting that SWNT material may have important applications in hydrogen storage. Theoretical calculations have had difficulty in reproducing the large H_2 wt% storage in SWNT bundles at room temperature. This underscores the necessity for more experiments which can provide details about gas–SWNT interactions.

The samples studied in this work were made on lightly compacted mats of tangled SWNT bundles ($\sim$1 mm $\times$ 2 mm $\times$ 0.1 mm). The material was obtained from Carbolex and consists of $\sim$50–70 vol% carbon as SWNTs. No post-synthesis chemical treatment was applied to the SWNT material used in these studies. Transmission electron microscopy (TEM) showed that the material consists of long bundles of SWNTs with mean bundle diameter $\sim$15 nm. Raman spectra, using a variety of excitation wavelengths, were similar to those reported earlier for arc-derived material [1,6]. The radial mode frequency (ω_r) has been found to exhibit a diameter (d) dependence of the form $\omega_r \sim 12 \pm 2\ \mathrm{cm}^{-1} + 224\ \mathrm{cm}^{-1}\ \mathrm{nm/d(nm)}$ [19]. The radial mode frequencies observed for these electric-arc-derived tubes indicate that the mean tube diameter is close to $\sim$1.4 nm. A small, ceramic-coated resistor placed near one end of the SWNT mat was used as a heater to induce a temperature difference $\Delta T < 0.5$ K along the length of the mat, as measured with two, type-K thermocouples. The corresponding thermoelectric voltage ΔV was also measured, and the thermoelectric power $S = \Delta V/\Delta T$ was computed. Four-probe ac resistance measurements used two additional Cu wires for current leads; two of the thermocouple arms provided the voltage leads. All leads and thermocouples made thermal and electrical contact to the mat with silver-loaded epoxy. Details of the 'analog subtraction' thermoelectric power measurement are available elsewhere [20,21]. Gas adsorption was studied using high purity (99.999%) gases (He, N_2, H_2, NH_3, O_2), and wt% gas uptake measurements were made in a turbo-pumped thermo-gravimetric analyzer (TGA; Hiden).

After in situ vacuum degassing at $T = 500$ K for $\sim$10 h in a vacuum of 10^{-8} Torr to remove O_2, the initial thermoelectric power S_0 of the mat exhibits a nearly linear T-dependence and is large and negative at room temperature ($-45\ \mu\mathrm{V/K} < S_0 < -40\ \mu\mathrm{V/K}$) [22,23]. This indicates that the mat behaves thermoelectrically as an n-type metal, and that S is dominated by the contribution from electrons in metallic tubes that form percolating conducting pathways through the sample. The thermoelectric response over time of this mat to 1 atm overpressure of He gas at $T = 500$ K (filled symbols) is shown in Fig. 2. The thermopower S is seen to exponentially rise with time (t), saturating at $\sim 12\ \mu\mathrm{V/K}$ above S_0. Removing the He overpressure above the mat induces an exponential decay of S with time (open symbols). The solid and dashed lines in the figure represent exponential fits to $S(t)$. Interestingly, the desorption time constant is $\sim$3 times larger than the adsorption time constant. The resistivity ρ for this He experiment (not shown in Fig. 2) was

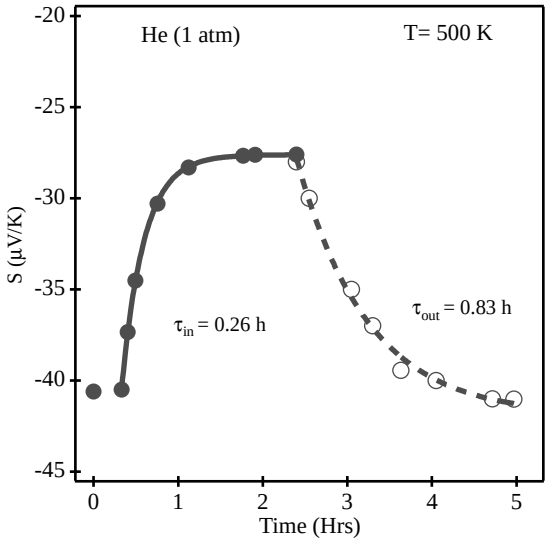

Fig. 2. The time-dependence of the response of the thermoelectric power S to a 1 atm overpressure of He gas (filled circles), and to the subsequent application of a vacuum over the sample (open circles). The time constant for the temperature variation is negligibly small.

found to exhibit a similar exponential rise and fall. A ~10% increase for ρ was observed due to He adsorption. These observations document a rather remarkable sensitivity of the thermoelectric transport parameters to adsorbed gases, even an inert gas such as He. Both S and ρ were completely reversible in these experiments.

In Fig. 3, we display S and ρ vs. P, the H_2 gas overpressure $(0 < P < 700$ Torr), for a similar SWNT mat at $T = 500$ K (the sample had been previously degassed as described above). Wt% hydrogen uptake (m) of a similar mat was measured in the TGA and plotted in the figure for comparison. All the data $(m,\ \rho,\ S)$ in Fig. 3 were collected after the samples were equilibrated at each pressure. We discuss the P-dependence of the wt% H_2 uptake first. For $P < 40$ Torr, the sample mass increases rapidly with increasing pressure, rising by ~0.5 wt% before rolling over at ~40 Torr, and thereafter increasing much more slowly over the remainder of the pressure range to ~700 Torr. We tentatively identify this behavior with the low-P filling of the highest energy binding site(s) which is complete at ~40 Torr. This site(s) should be the interstitial channel and/or the groove site(s)

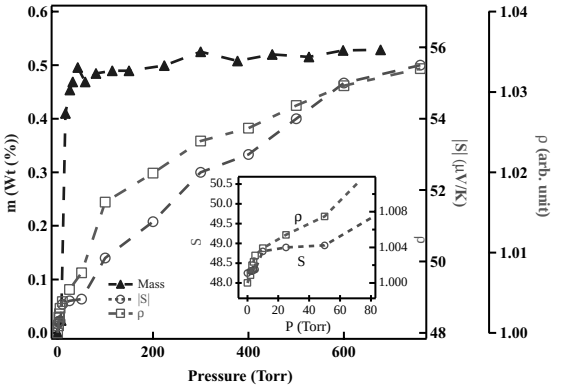

Fig. 3. Pressure-dependence $(0 < P < 750$ Torr) for wt% H_2 uptake (m), absolute value of the thermoelectric power $(|S|)$ and resistivity (ρ) in a SWNT mat. The structure near ~30–50 Torr in m, $(|S|)$, ρ is identified with the filling of the highest energy site in the bundle grooves or interstitial channels. The inset to the figure shows the $|S|$,ρ data at low pressure on an expanded scale; a clear knee or plateau is evident in the transport data near the pressure where the wt% H_2 uptake first saturates.

[13]. The subsequent slow rise in the wt% with increasing P above ~40 Torr is tentatively identified with the filling of the next higher energy site(s), i.e., the internal tube pores or external surface sites of the bundle. As can be seen in Fig. 3, and more clearly seen in the low-P inset to Fig. 3, both S and ρ exhibit a distinct knee, or short plateau at the same low pressure as m rolls over. Assuming our interpretation of the wt% H_2 uptake is indeed correct, it is clear that ρ and S are much more sensitive to the filling of the second, lower-energy site.

The thermoelectric response (S, ρ) of a bundle of SWNTs to a variety of gases (He, N_2, H_2, O_2 and NH_3) can be understood in terms of the change in the thermoelectric power of the metallic tubes due to either a charge-transfer-induced change of Fermi energy (i.e., molecule donates an electron to the conduction band) [24] or to the creation of an additional scattering channel for conduction electrons in the tube wall. This scattering channel is identified with impurity sites associated with the adsorbed gas molecules. We briefly develop the equations necessary to understand this point of view. We have argued earlier that the metallic behavior of the SWNT mat thermopower $(S \propto T)$ is a consequence of the

percolating pathways through the metallic tube components in the mat [23]. According to the Mott relation, the thermoelectric power associated with the diffusion of free carriers in a metal can be written compactly as a logarithmic energy derivative of the electrical resistivity (ρ) [25]

$$S = CT\frac{\mathrm{d}}{\mathrm{d}E}\{\ln\rho(E)\}_{E_F}, \tag{1}$$

where $C = (\pi^2 k_B^2/3|e|)$, k_B is Boltzmann's constant, T is the temperature, $\rho(E)$ is the energy-dependent resistivity, $|e|$ is the charge on the electron; the derivative is evaluated at the Fermi energy E_F. We next make a formal separation of the contributions to the total bundle resistivity from: (1) the scattering mechanisms pre-existing in the bundle before gas adsorption (ρ_0), e.g., from phonons and wall defects, and (2) the extra impurity scattering due to the adsorbed gas (ρ_a)

$$\rho = \rho_0 + \rho_a. \tag{2}$$

Eq. (2) expresses Matthiessen's rule, which is equivalent to the additive nature of independent scattering rates. It is usually understood that $\rho_0 \gg \rho_a$, i.e., the intrinsic resistivity is much greater than the additional resistivity due to impurities. This is certainly the case here, as verified by experiment. Substituting (2) into (1), and approximating $1/\rho \sim \rho_0^{-1}(1 - \rho_a/\rho_0)$, we find

$$S = S_0 + (\rho_a/\rho_0)(S_a - S_0), \tag{3}$$

where $S_j = CT\mathrm{d}/\mathrm{d}E(\ln\rho_j)_{E_F}$ for $j = (0, a)$, S_0 and S_a are, respectively, the contributions to the thermopower from the host resistivity $\rho_0(E)$ and the additional impurity resistivity $\rho_a(E)$ associated in the adsorbed gas. Eq. (3) was actually developed some time ago to discuss the thermoelectric behavior of Au and Ag alloys, and is known as the Nordheim–Gorter (N–G) relation [25]. If isothermal data S vs. ρ_a is linear, then Eq. (3) requires that the band structure and E_F of the host (Au), must be unaffected by the doping (Ge). That is S_0 and S_a must be constant. The spirit of the application of Eq. (3) to thermoelectric transport in nanotube bundles 'doped' with gas molecules is therefore clear. If the particular molecules under study are physisorbed, i.e., van der Waals bonded to the tube walls, they will induce only a small perturbation on the SWNT band structure, and an almost linear N–G plot should be obtained. If, on the other hand, the N–G plot for a particular adsorbed gas on SWNTs is strongly curved, this nonlinearity would indicate that the molecules are chemisorbed onto the tube walls. Chemisorption, of course, has a much more profound effect on the host band structure and/or the value of E_F, and thus $(S_a - S_0)$ must then depend on gas coverage or storage and the linearity of Eq. (3) with ρ_a is lost. N–G plots, therefore, should be very valuable in identifying the nature of the gas adsorption process in SWNTs.

In Fig. 4, we display the N–G plots (S vs. ρ_a) for isothermal adsorption of He, N_2, and H_2 in SWNTs at 500 K. As can be seen in the figure, the

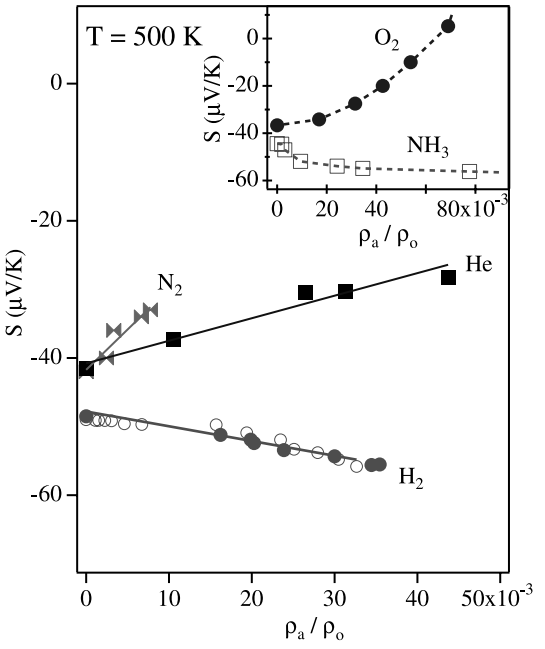

Fig. 4. N–G plots (S vs. ρ) showing the effect of gas adsorption on the electrical properties of the mat. Wt% gas stored in the bundle increases to the right, tracking the increase in ρ. A linear N–G plot indicates that physisorption is taking place (see text). For the H_2 data, the open circles are from the time dependent response to 1 atm of He at $T = 500$ K, and the closed circles are from a pressure study at $T = 500$ K. The intercepts on the S-axis of the data are different because S_0 varies slightly from sample to sample. The inset shows the N–G plots for O_2 (electron acceptor) and NH_3 (electron donor). The data in the inset are strongly curved indicating chemisorption is taking place.

data are linear for these three gases, indicating that these molecules physisorb on the SWNT surface. In the inset to Fig. 4, we display N–G plots for NH_3 and O_2; these are strongly curved, indicating, as discussed above, that these molecules must chemisorb on the tube walls. From past experience in carbons and polymers, NH_3 and O_2 act, respectively, as an electron donor and acceptor. Large changes in S and ρ [22,23] and FET channel conductance [24] have recently been reported for SWNTs exposed to O_2, and this has been identified with chemisorption [22–24]. Our N–G plot in Fig. 4 (inset) certainly confirms this point of view. Furthermore, recent theoretical calculations by Louie and co-workers [26] for O_2 on semiconducting SWNTs find significant electron transfer from the tube wall to the O_2 molecule (0.1 e per O_2), depressing E_F and rendering the material p-type.

Returning to the discussion of the linear N–G plots in Fig. 4 (for He, N_2, and H_2), some interesting points remain. First, the N–G slope for He and N_2 are positive, while that for H_2 is negative. According to (3), the sign of slope is determined by $(S_0 - S_a)$. Since $S_a \sim d/dE(\ln \rho_a)$, and recalling that this extra resistivity is proportional to the impurity scattering rate, a fundamentally different energy dependence for the electron scattering rate associated with He and H_2 adsorption sites must exist. We also note a significant difference in slope (but not sign) for He and N_2 sites as well. Indeed, it is the sensitivity of the N–G plots at fixed temperature to different molecules that can be the basis for the utility of a SWNT thermoelectric 'nano-nose'.

The sensitivity of S and ρ to coverage must be related to the quasi one-dimensional nature of the transport in SWNTs, and the fact that almost all carbon atoms are associated with one adsorption site or another. Theoretical calculations to investigate the scattering mechanism for various adsorption sites and molecules are now needed. As these calculations will have to deal with the details of the molecule–SWNT interaction, it is hoped that these calculations and the data presented here will provide quantitative insight into the details of the gas–SWNT interaction.

Acknowledgements

We thank V.H. Crespi, M.W. Cole, K.A. Williams for their valuable suggestions and discussions. This work was supported by ONR (ONR N00014-99-1-0619), NSF (UK MRSEC No. DMR 98-09686) and funding for H.E.R. by the Penn. State Materials Research Institute.

References

[1] M.S. Dresselhaus, G. Dresselhaus, P.C. Eklund, Science of Fullerenes and Carbon Nanotubes, Academic, San Diego, 1996.
[2] S. Iijima, T. Ichihashi, Nature 363 (1993) 603.
[3] D.S. Bethune, et al., Nature 363 (1993) 605.
[4] R. Thess, et al., Science 273 (1996) 483.
[5] K. Tanaka, T. Yamabe, K. Fukui, The Science and Technology of Carbon Nanotubes, Elsevier, Oxford, 1999.
[6] C. Journet, et al., Nature 388 (1997) 756.
[7] T.W. Odom, J.L. Huang, P. Kim, C.M. Liber, J. Phys. Chem. B 104 (2000) 2794.
[8] A. Ugawa, A.G. Rinzler, D.B. Tanner, Phys. Rev. B 60 (1999) R11305.
[9] S. Kazaoui, et al., Phys. Rev. B. 621 (2000) 643.
[10] R. Saito, G. Dresselhaus, M.S. Dresselhaus, Physical Properties of Carbon Nanotubes, Imperial College Press, Singapore, 1998.
[11] A.M. Rao, P.C. Eklund, A. Thess, R.E. Smalley, Nature 388 (1997) 257.
[12] R.S. Lee, H.J. Kim, J.E. Fischer, A. Thess, R.E. Smalley, Nature 388 (1997) 255.
[13] K.A. Williams, P.C. Eklund, Chem. Phys. Lett 320 (2000) 352.
[14] G. Stan, M.W. Cole, J. Low Temp. Phys 110 (1998) 539.
[15] A.C. Dillon, et al., Nature 386 (1997) 377.
[16] Y. Ye, et al., Appl. Phys. Lett. 74 (1999) 2307.
[17] C. Liu, et al., Science 286 (1999) 1127.
[18] M.J. Heben, private communication..
[19] M.S. Dresselhaus, P.C. Eklund, Adv. Phys. 49 (2000) 705.
[20] P.C. Eklund, A.K. Mabatah, Rev. Sci. Instrum. 48 (1977) 775.
[21] G.U. Sumanasekera, L. Grigorian, P.C. Eklund, Meas. Sci. Technol. 11 (2000) 237.
[22] P.G. Collins, K. Bradley, M. Ishigami, A. Zettl, Science 287 (2000) 1801.
[23] G.U. Sumanasekera, C.A.K. Adu, S. Fang, P.C. Eklund, Phys. Rev. Lett. 85 (2000) 1096.
[24] J. Kong, et al., Science 287 (2000) 622.
[25] R.D. Barnard, Thermoelectricity in Metal and Alloys, Wiley, New York, 1972.
[26] S.H. Jhi, S.G. Louie, M.L. Cohen, Phys. Rev. Lett. 85 (2000) 1710.